JOURNAL OF MAGNETIC RESONANCE **131,** 261–271 (1998)
ARTICLE NO. MN981367

Sensitivity Enhancement by Matched Microwave Pulses in One- and Two-Dimensional Electron Spin Echo Envelope Modulation Spectroscopy

G. Jeschke,[1] R. Rakhmatullin, and A. Schweiger

Laboratorium für Physikalische Chemie, Eidgenössische Technische Hochschule, CH-8092 Zürich, Switzerland

Received July 22, 1997; revised December 22, 1997

The concept of microwave pulse matching is applied to three-pulse electron spin echo envelope modulation and sublevel correlation (HYSCORE) spectroscopy. Matched pulses enhance the efficiency of forbidden transfers and may drastically increase the signal intensity of basic frequency and combination frequency transitions in these conventional pulse EPR experiments. The theory of matched pulses is extended to the case of strong and largely isotropic hyperfine interactions, and numerical simulations are presented to gain a deeper insight into the inner working of the matched-pulse approach. It is shown that the enhancement of combination frequencies in matched HYSCORE can be used to determine the relative sign of hyperfine coupling constants as well as the number of equivalent nuclei. The enormous capacity of the approach is demonstrated on ordered and disordered systems. In particular, it is shown that in HYSCORE experiments the signal-to-noise ratio improvement for strongly coupled nitrogens and for proton combination peaks may be considerably larger than one order of magnitude, corresponding to a reduction in measuring time of more than a factor of 100.

Key Words: **pulse EPR; ESEEM; matched pulses; HYSCORE; sensitivity enhancement.**

INTRODUCTION

One- and two-dimensional electron spin echo envelope modulation (ESEEM) experiments that rely on the free evolution of nuclear coherence are distinguished by a particularly high spectral resolution (*1–3*). The most frequently applied one-dimensional (1D) experiment of this type makes use of the three-pulse ESEEM sequence $\pi/2-\tau-\pi/2-T-\pi/2-\tau-$echo, with nonselective microwave (mw) pulses and a fixed time τ and variable time T (*1*). In this approach, in the following called ''standard'' three-pulse ESEEM, the modulation depth and thus the signal intensity of the nuclear frequency spectrum is determined solely by the spin system under consideration.

The most popular two-dimensional (2D) ESEEM experiment is HYSCORE (hyperfine sublevel correlation), introduced by Höfer *et al.* (*4*) and developed further by Höfer and others (*5–10*). HYSCORE makes use of the sequence $\pi/2-\tau-\pi/2-t_1-\pi-t_2-\pi/2-\tau-$echo, with a fixed time τ and variable times t_1 and t_2, incremented independently from each other. The mw π pulse applied at time t_1 after the second $\pi/2$ pulse transfers the nuclear coherences in one electron spin manifold to nuclear coherences in the other electron spin manifold. Standard HYSCORE again makes use of nonselective mw pulses, and the sensitivity of the approach is again determined solely by the spin system.

There is considerable interest in new experimental schemes for enhancing weak echo modulations by using building blocks better suited to the generation of nuclear coherence (*11–14*). A particularly promising approach makes use of matched or high-turning-angle (HTA) mw pulses for optimizing the generation and transfer of coherence (*15*). This is related to the matching of two radiofrequency fields for optimum coherence transfer in the rotating frame in heteronuclear NMR experiments (*16, 17*) and even more closely to a matching phenomenon in dynamic nuclear polarization experiments (*18, 19*). Recently, it has been demonstrated that the sensitivity of the two-pulse ESEEM experiment (*20*) can drastically be increased by matching the mw field strength with the nuclear Zeeman frequency.

In this paper, we introduce matched three-pulse ESEEM and matched HYSCORE. The two new experiments are distinguished by a considerable increase in the modulation amplitudes as compared to the corresponding standard approaches. For transitions between sublevels in one electron spin manifold that are connected via very weak forbidden EPR transitions with sublevels in the other electron spin manifold, the enhancement in signal intensity can *exceed one order of magnitude.* In particular the amplitudes of combination peaks that contain important information on the number of equivalent nuclei and on relative signs of hyperfine couplings are often drastically increased. We briefly recall the basics of the matched-pulse approach and give a theoretical description for the case of strong and largely isotropic hyperfine couplings.

[1] Present address: Max-Planck-Institute for Polymer Research, Postfach 3148, D-55021 Mainz, Germany.

1090-7807/98 $25.00

Then, we discuss the 1D and 2D matched experiment in some detail and illustrate the inner working by numerical simulations. Finally, the often overwhelming efficiency of the methods is demonstrated by experimental examples.

THEORY

Enhancement of Forbidden Transfers by Nonideal Microwave Pulses

Consider a simple model system consisting of one electron spin $S = 1/2$ and one nuclear spin $I = 1/2$. It has been shown earlier that the results obtained with such a system can easily be extended to systems with an effective electron spin $S > 1/2$ (*21*). The case of several nuclear spins will also be mentioned. The effective rotating frame Hamiltonian in the absence of an mw field can be written as

$$H_0 = \Omega_S S_z + \omega_I I_z + A S_z I_z + B S_z I_x, \qquad [1]$$

where $\Omega_S = \omega_S - \omega_{\mathrm{mw}}$ is the offset of the electron Zeeman frequency ω_S from the mw frequency ω_{mw}, ω_I is the nuclear Zeeman frequency, and A and B describe the secular and pseudo-secular part of the hyperfine coupling, respectively. In the same frame, the perturbation introduced by an mw field along the x axis is given by

$$H_{\mathrm{mw}} = \omega_{1S} S_x, \qquad [2]$$

with the mw field strength $\omega_1 = \gamma_e B_1$. In the eigenbasis of the unperturbed Hamiltonian H_0, H_{mw} can be expressed as

$$H_{\mathrm{mw}} = \omega_{1S} \cos\eta S_x + \omega_{1S} \sin\eta 2 S_y I_y. \qquad [3]$$

The first and second terms describe the perturbation of the allowed and forbidden transitions, respectively. In the tilted frame where the sum of the unperturbed Hamiltonian and of the perturbation of the *allowed* transitions is diagonal, the perturbation of the forbidden transitions is found to

$$\begin{aligned} H_{\mathrm{f}}^{\mathrm{eff}} = {} & \tfrac{1}{2}\omega_{1S} \sin\eta \cos\theta (S^+ I^- + S^- I^+) \\ & - \omega_{1S} \sin\eta \sin\theta I_x \\ & - \tfrac{1}{2}\omega_{1S} \sin\eta \cos\theta (S^+ I^+ + S^- I^-). \end{aligned} \qquad [4]$$

Details of the two frame transformations and the definitions of η and θ are given in (*15*) for the $S = 1/2$, $I = 1/2$ model system, and in (*21*) for an arbitrary spin S. As long as

$$\omega_{1S} \sin\eta \ll \tilde{\omega}_I, \qquad [5]$$

the second and third terms of Eq. [4] represent nonsecular terms that can be neglected. Here, $\tilde{\omega}_I$ is the effective nuclear Zeeman frequency that is equal to half the splitting between the two forbidden transitions in the ESR spectrum. Maximum mixing between electron and nuclear spins occurs when the first term in Eq. [4] connects degenerate levels, i.e., at the matching condition (*15, 21*)

$$\omega_{1S}^{\mathrm{m}} = \frac{1}{|\tilde{\omega}_I| \cos\eta} [\omega_{12}\omega_{34}(\tilde{\omega}_I^2 - \Omega_S^2)]^{1/2}, \qquad [6]$$

where ω_{12} and ω_{34} are signed nuclear frequencies with absolute values given by

$$|\omega_{12}| = \left[\left(\omega_I + \frac{A}{2} \right)^2 + \frac{B^2}{4} \right]^{1/2}, \qquad [7a]$$

$$|\omega_{34}| = \left[\left(\omega_I - \frac{A}{2} \right)^2 + \frac{B^2}{4} \right]^{1/2}. \qquad [7b]$$

The sign of their product is positive in the weak coupling case, $|A| < 2|\omega_I|$, and negative in the strong coupling case, $|A| > 2|\omega_I|$. For small hyperfine couplings and resonance offsets, A, $\Omega_S \ll \omega_I$, Eq. [6] reduces to

$$\omega_{1S}^{\mathrm{m}} \approx \omega_I. \qquad [8]$$

Under this condition, ω_{1S} can be tuned close to optimum electron-nuclear spin mixing even for moderate hyperfine couplings, since the exact matching condition depends on the resonance offset Ω_S that usually features a broad distribution in an ESR spectrum. Due to the small mixing term in Eq. [4], optimization of the forbidden transfers also requires longer mw pulses; i.e., flip angles much larger than $\pi/2$ and π must usually be applied (*15*). As a rule of thumb, the time scale of the coherence transfer from electron to nuclear spins, or vice versa, should be close to $\pi/(2\omega_{1S}\sin\eta)$. In practice, the optimum pulse length also depends on relaxation times and on destructive interference of spin packets with different Ω_S.

For $|A| \gg 2|\omega_I|$, the above treatment fails, since for ω_{1S}^{m} defined by Eq. [6], condition [5] is no longer fulfilled even for small $\sin\eta$. For the theoretical description of this important case, the additional assumption $B \ll A$ must be made, which holds, for example, for hyperfine couplings of central ions in a variety of transition metal complexes or for directly coordinated nitrogens in a copper complex (dominating Fermi contact term). Using $\sin\eta \ll 1$, a unitary transformation with the propagator $U = \exp\{-i(\theta_\alpha S_y I^\alpha + \theta_\beta S_y I^\beta)\}$ leads to a tilted frame, where $H_0 + H_{\mathrm{mw}}$ can be written as

$$\begin{aligned} H^{(1)} = {} & \Omega_S^{(1)} S_z + \omega_I I_z + A^{(1)} S_z I_z \\ & + B \cos\theta^{(1)} S_z I_x + B \sin\theta^{(1)} S_x I_x, \end{aligned} \qquad [9]$$

with $\theta^{(1)} = (\theta_\alpha + \theta_\beta)/2$ and

$$\theta_\alpha = \text{atan}\left(\frac{-\omega_{1S}}{A/2 + \omega_I}\right), \quad [10a]$$

$$\theta_\beta = \text{atan}\left(\frac{\omega_{1S}}{A/2 - \omega_I}\right). \quad [10b]$$

The effective resonance offset $\Omega_S^{(1)}$ and effective hyperfine coupling $A^{(1)}$ are given by

$$\Omega_S^{(1)} = (\omega_{13}^{(1)} + \omega_{24}^{(1)})/2, \quad [11a]$$

$$A^{(1)} = (\omega_{13}^{(1)} - \omega_{24}^{(1)}), \quad [11b]$$

with the perturbed ESR frequencies

$$\omega_{13,24}^{(1)} = \left(\Omega_S \pm \frac{A}{2}\right)\cos\theta_{\alpha,\beta} - \omega_{1S}\sin\theta_{\alpha,\beta}. \quad [11c]$$

Since $B \ll A$, the term $B \cos\theta^{(1)} S_z I_x$ is nonsecular and can be neglected. The term $B \sin\theta^{(1)} S_x I_x$ connects state $|\alpha, \alpha\rangle$ with $|\beta, \beta\rangle$ (double-quantum transition) and state $|\alpha, \beta\rangle$ with $|\beta, \alpha\rangle$ (zero-quantum transition). The former part is also nonsecular, while the latter part again leads to maximum electron-nuclear spin mixing, if the states $|\alpha, \beta\rangle$ and $|\beta, \alpha\rangle$ are degenerate. The matching condition is then given by

$$\omega_{1S}^{m} = [(A^2/4 - \omega_I^2)(\Omega_S^2 - \omega_I^2)]^{1/2}/|\omega_I|, \quad [12]$$

which can alternatively be written as

$$|\Omega_S^{m}| = |\omega_I| \frac{(A^2/4 + \omega_{1S}^2 - \omega_I^2)^{1/2}}{(A^2/4 - \omega_I^2)^{1/2}}. \quad [13]$$

According to Eq. [12], matching is only possible for spin packets with $\Omega_S > \omega_I$. For an optimum coherence transfer it is also necessary to maximize $\sin\theta^{(1)}$, since the magnitude of the off-diagonal element $B \sin\theta^{(1)} S_x I_x$ determines both the matching range with respect to Ω_S and the rate of the coherence transfer. In contrast, for the case of weak or moderate couplings treated above, the mixing term is proportional to $\cos\theta$ and does *not critically* depend on ω_{1S} for spin packets that are strongly excited. For the present case, there are always spin packets for which the matching condition [13] is fulfilled, as long as the distribution of Ω_S is broad compared to the maximum available mw field $\omega_{1S}^{\max}$. Furthermore, we find

$$\sin(2\theta^{(1)}) = \frac{\omega_{1S}\Omega_S}{|\omega_{13}\omega_{24}|}, \quad [14a]$$

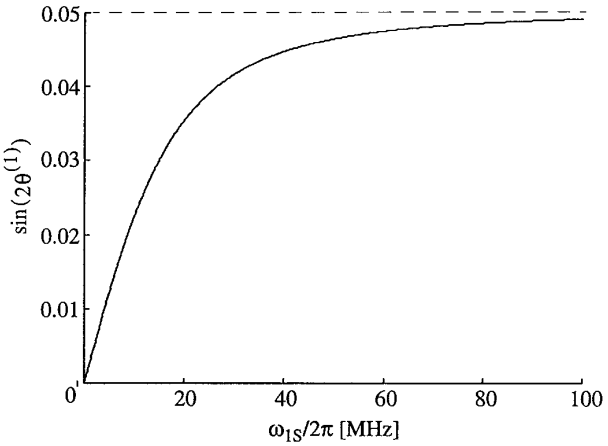

FIG. 1. Dependence of $\sin(2\theta^{(1)})$ (cf. Eqs. [9]–[15]) on the mw field strength ω_{1S} for $A/2\pi = 40$ MHz, $\omega_I = 1$ MHz. The mixing term between electron and nuclear spins for nuclei with $A \gg \omega_I$ is proportional to $\sin(\theta^{(1)})$. The dashed line indicates the asymptotic value.

with

$$|\omega_{13}| = \sqrt{(\Omega_S + A/2)^2 + \omega_{1S}^2}, \quad [14b]$$

$$|\omega_{24}| = \sqrt{(\Omega_S - A/2)^2 + \omega_{1S}^2}. \quad [14c]$$

From Eqs. [13] and [14a] one finds that for a given Ω_S^{m}, $\sin\theta^{(1)}$ increases monotonically with ω_{1S}, with the asymptotic value

$$\lim_{\omega_{1S}\to\infty} \sin(2\theta^{(1)}) = \frac{2\omega_I(A^2 - 4\omega_I^2)^{1/2}}{A^2}. \quad [15]$$

This is shown in Fig. 1 for a typical parameter set ($A/2\pi = 40$ MHz, $\omega_I/2\pi = 1$ MHz). In addition, the derivatives with respect to Ω_S of both $\sin\theta^{(1)}$ and the energy difference between the states $|\alpha, \beta\rangle$ and $|\beta, \alpha\rangle$ *decrease* monotonically with increasing ω_{1S}. This reinforces a broadening of the matching region. For an infinitely broad inhomogeneous line one therefore expects *optimum sensitivity with the largest achievable mw field*. This is true for most practical situations, since the ESR linewidth is usually larger than $\omega_{1S}^{\max}$.

Sensitivity enhancement in cases with strong, mainly isotropic hyperfine couplings does therefore not require a matching of the mw field. However, as in cases with weak and moderate couplings, the coherence transfer between electron and nuclear spins occurs on a time scale that is much longer than $1/\omega_{1S}$. Note that the qualitative conclusions of this treatment given for $I = 1/2$ can also be applied to larger nuclear spins, since in cases with strong hyperfine coupling the quadrupole interaction is usually much smaller than both the hyperfine coupling and $\omega_{1S}^{\max}$. Numerical simulations that corroborate this reasoning will be shown below.

TABLE 1
Coherence Transfer Pathways Leading to Nuclear Modulation in Three-Pulse ESEEM

No.	First transfer	First evolution	Second transfer	Second evolution	Third transfer	Third evolution	Detection
1	Allowed	aEC	Forbidden	NC	Forbidden	aEC	Allowed
2	Forbidden	fEC	Allowed	NC	Forbidden	aEC	Allowed
3	Allowed	aEC	Forbidden	NC	Allowed	fEC	Forbidden
4	Forbidden	fEC	Allowed	NC	Allowed	fEC	Forbidden

Note. aEc, allowed electron coherence; fEC, forbidden electron coherence; NC, nuclear coherence.

Matched Three-Pulse ESEEM and HYSCORE

It has been shown earlier that matched-pulse ESR experiments require an analysis of the coherence transfer pathways in terms of allowed and forbidden transfers (*20*). In this classification, allowed transfers are those that do not change the nuclear spin state, while forbidden transfers correspond to a $\pi/2$ pulse, and doubly forbidden transfers to a π pulse applied to the nuclear spins. Since three-pulse ESEEM is an experiment where nuclear coherence is both created and indirectly detected, it necessarily features *two* forbidden processes, where a forbidden process is either a forbidden transfer or the detection of forbidden electron coherence. The character of the transfer and the type of coherence during the free evolution periods of the three-pulse experiment are summarized in Table 1 for the four coherence transfer pathways that contribute to the modulation. The *T*-independent and thus unmodulated part of the stimulated echo is not considered, since for the observation of modulations this part of the echo is of no relevance. Rather, the unmodulated part is a nuisance in three-pulse ESEEM and HYSCORE experiments, and since the formation of this echo follows a coherence transfer pathway with only allowed processes, it is at least partially suppressed by matching.

The detection of forbidden electron coherence at the end of the pulse sequence cannot be improved by pulse matching (so-called detection bottleneck (*20*)). This limits the enhancement of pathways 3 and 4 (Table 1), so that only the enhancement of pathways 1 and 2 must be considered. For pathway 1, the second and third pulses should be matched and extended, and for pathway 2 the first and third pulses. Matching a pulse for an *allowed* transfer deteriorates the signal. This is because enhancing forbidden transfers necessarily diminishes allowed transfers. The loss in signal intensity due to all these undesired effects is expected to be larger than a factor of 2 under optimum matching conditions. As a consequence enhancing only one of the two pathways 1 or 2 by two HTA pulses leads to better results than matching all three pulses. The two sequences that enhance pathways 1 and 2 are shown in Figs. 2a and 2b. For any particular set of *A* and *B* they are theoretically equivalent inspite of the fact that in pathway 2 the electron coherence defocuses on forbidden and refocuses on allowed transitions. This asymmetry leads to a phase shift in the nuclear modulation which in disordered systems might result in additional destructive interference between orientations with different *A* and *B* values. Although a detailed investigation of such effects is beyond the scope of this paper, we prefer in the following the more symmetric pulse sequence that enhances pathway 1.

The conclusions from this analysis of the coherence transfer pathways have been verified by numerical simulations performed with the software package GAMMA (*22*). As a parameter set we used values typical for weakly coupled protons in transition metal complexes and organic radicals: $\omega_I/2\pi = -14$ MHz; $A/2\pi = 1.68$, $B/2\pi = 0.92$ MHz. An interpulse delay of $\tau = 175$ ns was used for minimum suppression of the two nuclear frequencies in standard (hard-pulse) three-pulse ESEEM; relaxation was neglected. An inhomogeneously broadened Gaussian-shaped ESR line with a full width at half-height of $\Gamma_{inh} = 20$ MHz was assumed.

The dependence of the line intensity of the ω_{12} transition

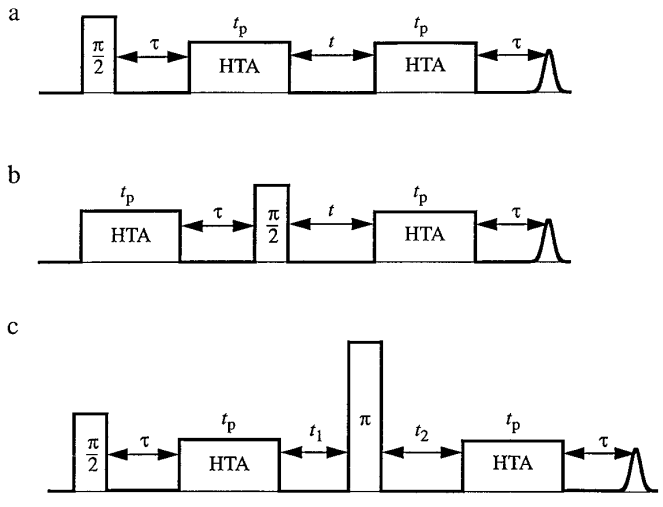

FIG. 2. Pulse sequences for matched three-pulse ESEEM and HYSCORE. HTA, matched high-turning-angle pulse. (a) Three-pulse ESEEM sequence for enhancing pathway 1 in Table 1. (b) Three-pulse ESEEM sequence for enhancing pathway 2. (c) HYSCORE sequence for enhancing pathway 1.

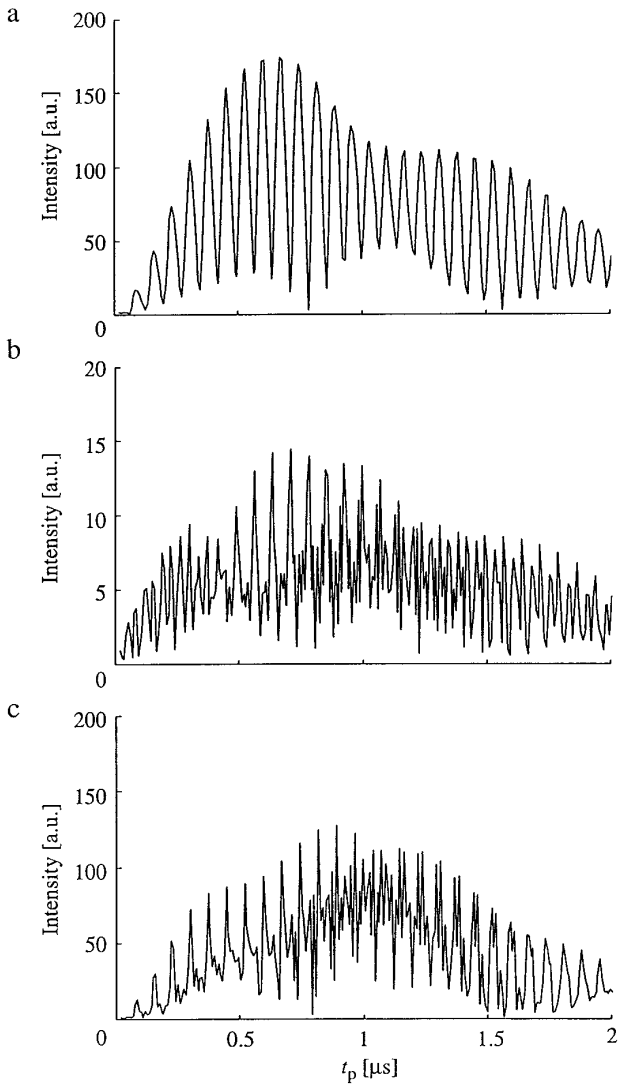

FIG. 3. Intensity of the ω_{12} transition as a function of the length t_p of the matched pulses in three-pulse ESEEM. (a) The second and third pulses are matched (cf. Fig. 2a). (b) The first and second pulses are matched (note the different vertical scale). (c) All three pulses are matched.

on the length of the matched pulses for three types of matched three-pulse ESEEM experiments is shown in Fig. 3. The intensity of the ω_{34} transition shows a similar behavior. The intensity found in the corresponding standard three-pulse ESEEM with $\pi/2$ pulses is close to the one observed with $t_p = 18$ ns (first data point in Fig. 3). By matching the second and third pulses (enhancement of pathway 1), we find a gain in signal amplitude of a factor of 50 at pulse lengths of about 600 ns (see Fig. 3a). The enhancement factor oscillates approximately with ω_{1S}, a behavior that is expected to be less pronounced in practice, because mw field inhomogeneities lead to a distribution of the ω_{1S} values. A result that is only slightly inferior is obtained by matching the first and third mw pulses (enhancement of pathway 2, data not shown). The difference may be traced back to sampling effects and is not significant. If only one of the three pulses is matched, the gain in signal amplitude is reduced to a factor of less than 5 (data not shown). Matching the first and second pulses to optimize the two pathways with the detection bottleneck is also distinguished by a small enhancement (Fig. 3b). Finally, matching of all three pulses leads to a deterioration as compared to enhancing only two forbidden transfers (Fig. 3c). Note that this deterioration becomes even worse when relaxation is considered.

To verify the theoretical predictions on the enhancement of modulation depths of strongly coupled nuclei, a simulation was performed with an $I = 1$ nucleus and a parameter set typical for directly coordinated nitrogens in a copper complex: $\omega_I/2\pi = 1$ MHz; $A/2\pi = 41.87$, $B/2\pi = 1.92$, quadrupole splitting $\omega_Q/2\pi = 0.62$, $\Gamma_{inh} = 200$ MHz; $\tau = 80$ ns. The pulse sequence with an extended second and third pulse ($t_p = 1$ μs) shown in Fig. 2a was used and the strength of the mw field was varied from 0 to 150 MHz. In agreement with theoretical predictions, we find that the intensity increases in general with increasing mw field (data not shown). Note however that the optimum length of the extended pulses also depends on the mw field strength. We may thus conclude that maximum enhancement is obtained by using the maximum mw field and optimizing τ and t_p.

Three-pulse ESEEM can be extended to the two-dimensional HYSCORE experiment, which correlates nuclear frequencies in the two electron spin manifolds by inserting an mw π pulse between the second and third mw $\pi/2$ pulses and incrementing the second and third interpulse delays separately (*4*). The coherence transfer pathways in this experiment are well understood (*7*) and several incrementation schemes have been proposed for this sequence, like DEFENCE (*8*), or a one-dimensional ESEEM-based version of hyperfine spectroscopy (*9*). In all these experiments, matching can be used to improve sensitivity. The additional π pulse that inverts the electron spin state accomplishes an allowed nuclear coherence transfer; the π pulse should therefore be neither matched nor extended. The sequence for matched HYSCORE is shown in Fig. 2c. To minimize artifacts along the diagonal, a π pulse of the same length as the hard $\pi/2$ pulse was used.

Combination Peaks in HYSCORE: Determination of Equivalent Nuclei and Relative Signs of Hyperfine Couplings

Strong enhancements of combination lines between several nuclei have already been observed in matched two-pulse ESEEM (*15*). Later, a detailed theoretical description of the effects of nonideal pulses on multispin systems was given (*20*); we therefore only recall the most important conclusions. Since for weak coupling the matching field is close to the nuclear Zeeman frequency, we consider systems with

several nuclei of the same isotope. Furthermore, we are interested in the simultaneous matching of single-quantum transitions ($k = 1$) rather than in a *direct* matching of multiple-quantum transitions that is maximum for $\omega_1^{m(k)} \approx k\omega_I$ with $k > 1$. It has been shown that even for this simple case the product rule for ESEEM intensities breaks down (*20*). Nevertheless, this rule can still be considered a zero-order approximation that allows for some qualitative insight. This is particularly true as long as the ''flip angle'' for the nuclear spins still fulfills the linear regime approximation. In practice, one is often forced to work in this regime since relaxation and destructive interference of spin packets do not allow the use of long excitation times necessary to obtain a complete transfer. Matching can be considered a method for increasing the flip angle of nuclear spins with respect to the value η obtained with hard pulses. In the linear regime, the amplitude of coherences involving n nuclear spins is given by

$$c_n = C \prod_{i=1}^{n} \beta_i , \qquad [16]$$

where C is a constant and the β_i are the flip angles of the n nuclear spins. On the other hand, the amplitude of the ith single-quantum coherence is proportional to β_i. Since pulse matching increases all the β_i simultaneously, a gain G for a single-quantum coherence translates into a gain of roughly G^n for a multiple-quantum coherence involving n spins. Therefore, multiple-quantum correlation peaks in HYSCORE are distinguished by a *larger* enhancement factor than single-quantum correlation peaks. At first sight, one might expect that the multiple-quantum correlation peaks complicate the spectra. However, for weak couplings the peaks representing k-quantum coherence are centered around $k\omega_I$ and are usually well separated from each other. Multiple-quantum peaks can then be used to get information on the spin system that cannot be obtained from single-quantum correlation peaks.

In ESEEM spectroscopy it is rather difficult to deduce any information on the number of equivalent nuclei in ordered systems, or on the number of nuclei of a particular isotope in the close vicinity of a paramagnetic center in a disordered system. Methods that attempt to solve this problem usually rely on the modulation depth (*23–25*). However, this approach is not model-free and ignores effects of pulse nonideality as well as differences in relaxation of the various coherence transfer pathways. In many practical cases, the agreement between experimental and simulated time traces is therefore not satisfying. In contrast, the observation of multiple-quantum correlation peaks of order k necessarily implies that at least k nuclei of a given isotope are in the vicinity of the paramagnetic center. In addition, the frequencies of these cross peaks contain information on the sum of hyperfine couplings that can also be used to determine relative signs of hyperfine couplings, since in three-pulse ESEEM

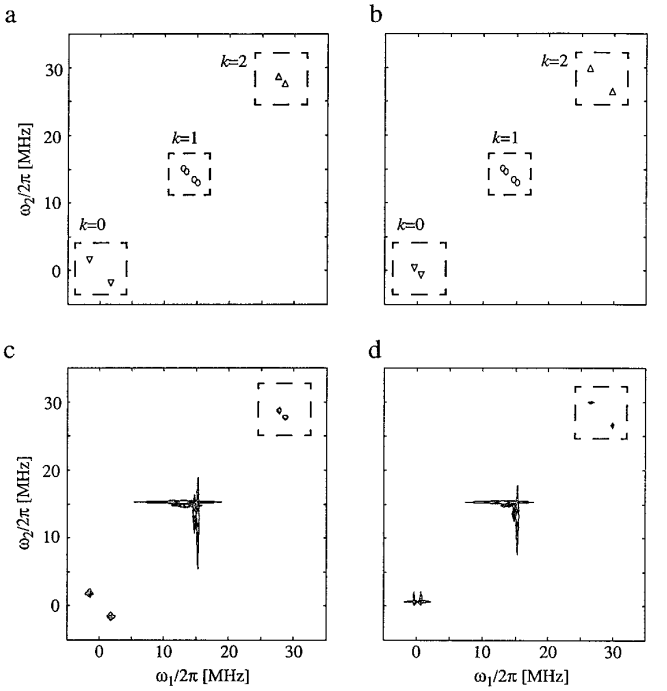

FIG. 4. Determination of relative signs of hyperfine couplings with matched HYSCORE. k designates the order of the multiple-quantum coherence that leads to the correlation peaks. (a) Schematic contour plot for parameter set I. (b) Schematic contour plot for parameter set II. (c) Numerical simulation, parameter set I with $\tau = 175$ ns, $\Gamma_{inh} = 20$ MHz, and $t_p = 674$ ns. (d) Numerical simulation, parameter set II.

and HYSCORE the cross peaks do not correlate nuclear frequencies in the *same* electron spin manifold. This is illustrated by the schematic 2D plots in Fig. 4 for the three-spin system $S = 1/2$, $I_1 = 1/2$, $I_2 = 1/2$ with parameter set I: $\omega_I/2\pi = -14$ MHz; $A_1/2\pi = 2.18$, $A_2/2\pi = -1.18$, $B_1/2\pi = 1.12$, $B_2/2\pi = -0.72$ MHz (Fig. 4a); and parameter set II: $\omega_I/2\pi = -14$ MHz; $A_1/2\pi = 2.18$, $A_2/2\pi = 1.18$, $B_1/2\pi = 1.12$, $B_2/2\pi = 0.72$ MHz (Fig. 4b). As an example, the double-quantum cross peaks ($k = 2$) correlate the combination frequency consisting of $\omega_{\alpha j}$ and $\omega_{\alpha I}$, with the combination frequency consisting of $\omega_{\beta j}$ and $\omega_{\beta I}$. To first order, the splitting between the two frequencies is $A_j + A_I$. The *absolute* values of A_j and A_I can be obtained by analyzing the single-quantum region of the HYSCORE spectrum. The occurrence of double-quantum peaks with a splitting of $|A_j| - |A_k|$ then implies that the two hyperfine couplings are different in sign (Fig. 4a), while peaks with a splitting of $|A_j| + |A_k|$ imply the same sign (Fig. 4b).

Numerical simulations of matched HYSCORE with the sequence shown in Fig. 2c have been performed with the same two parameter sets and $\tau = 175$ ns, $\Gamma_{inh} = 20$ MHz, and $t_p = 674$ ns. The result shown in Figs. 4c and 4d confirms the peak positions of the schematic plots. In the simulation with hyperfine couplings of the same sign also diagonal peaks at $(\omega_{\alpha j} - \omega_{\alpha I}, \omega_{\alpha j} - \omega_{\alpha I})$ and $(\omega_{\beta j} - \omega_{\beta I}, \omega_{\beta j} - \omega_{\beta I})$

are found. Moreover, comparison with a simulated standard HYSCORE spectrum (not shown) also confirms that the multiple-quantum peaks in matched HYSCORE are enhanced with respect to the single-quantum peaks. Note that the occurrence of either of these combinations proves that the two nuclei are coupled to the same electron spin, a fact that is of importance when the ESR spectra of different paramagnetic centers overlap. Multiple-quantum HYSCORE thus contains the same information as the TRIPLE experiment in ENDOR spectroscopy (*26, 27*).

For the determination of relative signs of hyperfine couplings by HYSCORE spectroscopy, it has been proposed earlier to use correlation peaks between $\omega_{\alpha j}$ and $\omega_{\beta I}$, or $\omega_{\alpha I}$ and $\omega_{\beta j}$. However, since the transfer of such cross peaks by the π pulse is *doubly forbidden,* they can be observed only in cases where at least one of the nuclei features a large modulation depth (*4, 28*). In principle, it is possible to enhance such peaks and simultaneously diminish the usual correlation peaks by matching the π pulse. However, the correlation of $\omega_{\alpha j}$ with $\omega_{\alpha I}$, and $\omega_{\beta j}$ with $\omega_{\beta I}$, is also doubly forbidden, so that a matched pulse no longer guarantees inversion of the electron spin state. In addition, all these peaks are close to the allowed single-quantum correlation peaks and it may be difficult to detect them if the couplings are small. We therefore propose multiple-quantum HYSCORE for sign determination.

EXPERIMENTAL

All experiments have been performed on a Bruker ESP 380E spectrometer equipped with the dielectric resonator probeheads ER 4118 and EN 4118, and with a cryogenic system from Oxford Instruments. In the standard three-pulse ESEEM and HYSCORE experiment all the pulses had a length of 16 ns. For the ''hard'' $\pi/2$ pulses and the matched pulses for the weak coupling case (proton enhancement), the amplitude of the mw field was adjusted by maximizing the two-pulse echo with 16- and 32-ns pulses. This condition corresponds to $\omega_{1S}/2\pi = 15.6$ MHz, a value that was found to be sufficiently close to the matching field $\omega_{1S}^{m}/2\pi$ for proton Zeeman frequencies in the range 12–15 MHz. In order to match the transfer of strongly coupled nuclei (nitrogen), the maximum available mw field of about $\omega_{1S}/2\pi =$ 30 MHz was used. Echo signals were integrated over a gate width of 24 ns in the standard pulse sequences and over 32–40 ns in the matched experiments. Four- and eight-step phase cycles (*7*) were applied for three-pulse ESEEM and HYSCORE experiments, respectively. All measurements were performed at 15 K.

As a disordered model system, we used the interphase layer between a thiokol-expoxy polymer adhesive and brass (60% copper) hitherto be referred to as the ''glue.'' It has been shown before that in this sample protons are only weakly coupled to a copper(II) center (*29*). All measurements on the glue were performed at the ESR signal maximum ($B_0 = 343$ mT). As an ordered model system, we used a single crystal of nickel(II)salicylaldoximate, $Ni(sal)_2$, doped with $Cu(sal)_2$ (*30*). All measurements on this sample were performed at the same arbitrary crystal orientation, with $B_0 = 290.9$ mT, and $\omega_{mw}/2\pi = 9.753$ GHz.

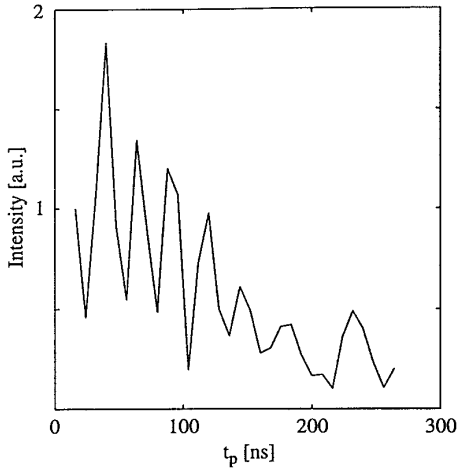

FIG. 5. Dependence of the proton line intensity on the pulse length t_p in proton-matched three-pulse ESEEM on a copper-containing expoxy glue.

RESULTS AND DISCUSSION

Three-Pulse ESEEM

To exclude signal enhancements in going from the standard to the matched experiment caused by the suppression effect, we first optimized the value of the interpulse delay τ by performing a 2D three-pulse ESEEM experiment with the sequence $16(\pi/2)-\tau-16(\pi/2)-T-16(\pi/2)-\tau-$ echo, and the time variables T and τ. With a starting value $\tau_0 = 120$ ns, the signal was found to be maximum at $\tau = 144$ ns for both samples. With this τ value we then performed 2D proton- and nitrogen-matched three-pulse ESEEM experiments, $16(\pi/2)-\tau-\text{pulse}(t_p)-T-\text{pulse}(t_p)-\tau-\text{echo}$, with a variable T and t_p ($\Delta t_p = 8$ ns).

The dependence of the amplitude of the matrix proton line on t_p in matched three-pulse ESEEM of the glue is shown in Fig. 5. Compared to standard three-pulse ESEEM ($t_p =$ 16 ns), a nearly twofold increase in signal amplitude is found for $t_p = 40$ ns. Note that with increasing pulse length also a line at twice the proton frequency can be observed. This is supported by theory that predicts a strong enhancement for the generation and detection of double-quantum nuclear coherence (data not shown). Additional local maxima at which the lines are also more intense than in standard three-pulse ESEEM are found at $t_p = 64$ and 88 ns.

The corresponding 2D three-pulse ESEEM experiments on $Cu(sal)_2$ are shown in Fig. 6. With proton matching (Fig.

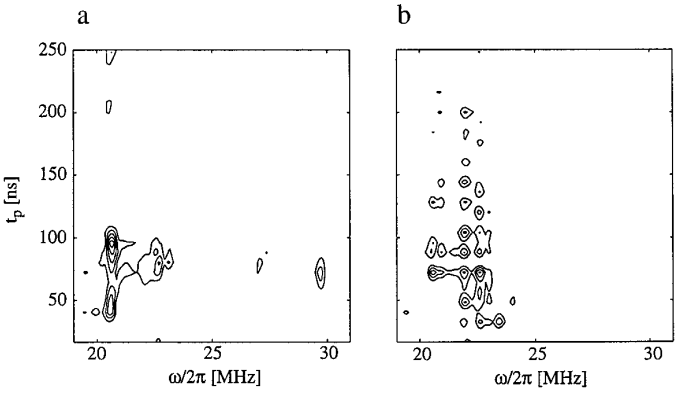

FIG. 6. Dependence of proton- and nitrogen-matched three-pulse ESEEM of bis(salicylaldoximato)Cu(II), $Cu(sal)_2$, doped into a single crystal of the corresponding nickel complex, on the length t_p of the second and third mw pulse. (a) Proton-matched three-pulse ESEEM with $\omega_{1S}/2\pi \approx \omega_I/2\pi = 14.7$ MHz, $\tau = 144$ ns. Proton double-quantum transitions between 20 and 30 MHz are enhanced. (b) Nitrogen-matched three-pulse ESEEM: $\omega_{1S}/2\pi \approx 30$ MHz, $\tau = 136$ ns. Transitions of the strongly coupled nitrogens are enhanced.

6a), proton double-quantum lines between 20 and 30 MHz can be observed. With an mw field of 30 MHz (nitrogen matching), the intensity of these proton lines again drops below the noise level and strong nitrogen peaks are observed instead (Fig. 6b). Further evidence for this line assignment is obtained from the HYSCORE spectra (see below). To the best of our knowledge, this is the first observation of a strongly coupled nitrogen with $A/2\pi > 30$ MHz by an ESEEM method. An optimum pulse length of $t_p = 72$ ns for both proton and nitrogen matching can be inferred from these plots, corresponding to a nominal flip angle of $\frac{9}{4}\pi$ for the protons and $\frac{9}{2}\pi$ for the nitrogens. The optimum flip angle of the matched pulses for the weakly coupled protons is only slightly larger than 2π. Although the τ value corresponding to a minimum suppression effect in standard three-pulse ESEEM was generally found to be satisfactory also for matched ESEEM, we repeated the matched three-pulse ESEEM experiment with different τ values. For protons, the same optimum τ values were found for both the standard and the matched experiment, whereas for nitrogens, a value of $\tau = 136$ ns proved to give slightly larger signal amplitudes in nitrogen-matched ESEEM.

HYSCORE

HYSCORE experiments were performed with several τ values, because the suppression of one of the two correlated ESEEM frequencies also suppresses the corresponding cross peak. Since the two correlated nuclear frequencies are usually not known, it is in general not possible to infer an optimum τ value from the 2D three-pulse ESEEM experiment. A standard and a proton-matched HYSCORE spectrum of the glue are shown in Fig. 7. The experimental conditions were the same in both cases except for the lengths of the second and fourth mw pulses. Besides a slightly enhanced peak close to the proton Zeeman frequency ω_{IH}, a strong double-quantum proton peak close to (30, 30) MHz is observed in the matched HYSCORE spectrum (Fig. 7b). From the shape of this peak we can infer that the proton hyperfine couplings are at least 1 MHz. Furthermore, the width of the double-quantum peak along the antidiagonal is roughly the same as the width of the single-quantum peak, implying that at least two protons with a coupling of this order of magnitude must be present.

Standard single-crystal proton- and nitrogen-matched HYSCORE spectra of $Cu(sal)_2$ are shown in Fig. 8. The sequence $16(\pi/2)-\tau-72(\mathrm{HTA})-t_1-16(\pi)-t_2-72(\mathrm{HTA})-\tau-$echo was used for both matched experiments. The τ values were taken from the 2D matched three-pulse ESEEM, since the information about the correlation of the single-quantum peaks could easily be inferred from these spectra. The same contour levels are used in all three spectra. Note the large number of proton combination peaks that can be observed with proton matching (Fig. 8b) and the drastic increase in signal intensity of the nitrogen peaks observed with nitrogen matching (Fig. 8c). Regions of particular interest are shown in more detail in Figs. 9–11.

Figure 9 shows the first quadrant and part of the second quadrant of the proton-matched HYSCORE plot in more detail. In contour plots with a large intensity ratio between the different peaks, ridges of the strong Lorentzian-shaped cross peaks parallel to the frequency axes (star effect) may become a severe problem. To remove these undesirable ridges we therefore made use of a Lorentz–Gauss transformation which converts the exponential decay into a Gaussian envelope by means of a proper weighting function. The contours become then circular for equal and elliptical for unequal linewidth in the two dimensions (*31*). The contour

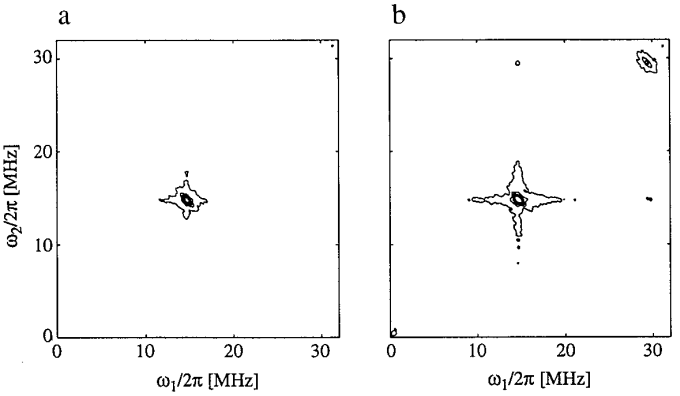

FIG. 7. Matched HYSCORE spectra of a copper-containing epoxy glue. (a) Standard HYSCORE, pulse sequence $16-\tau-16-t_1-16-t_2-16-\tau-$echo, $\tau = 152$ ns. (b) Proton-matched HYSCORE, pulse sequence $16-\tau-88(\mathrm{HTA})-t_1-16-t_2-88(\mathrm{HTA})-\tau-$echo, $\tau = 152$ ns.

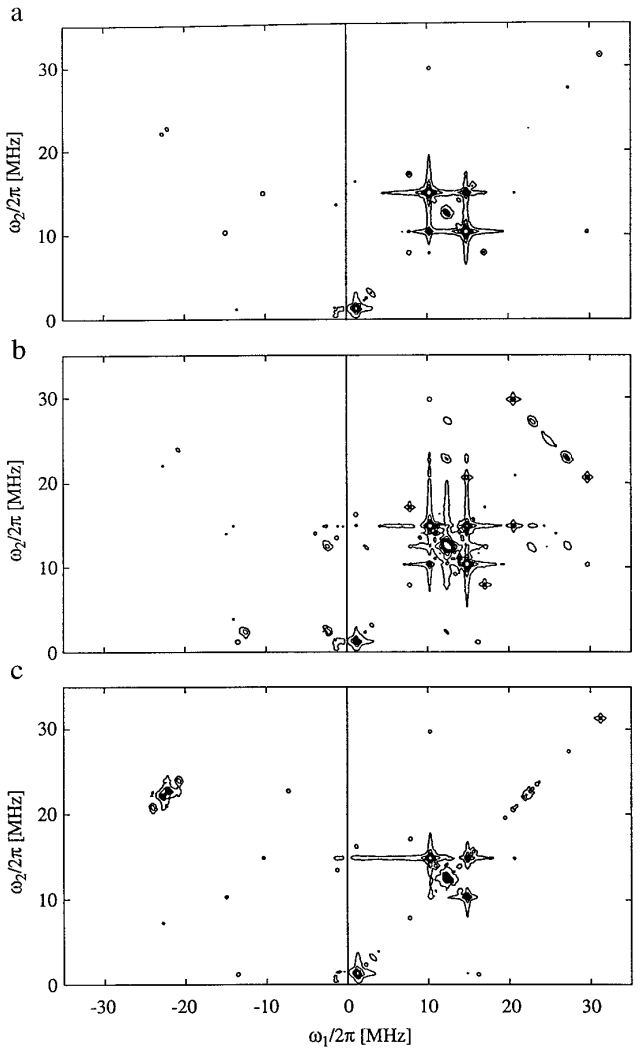

FIG. 8. Single-crystal HYSCORE spectra of $Cu(sal)_2$. The same contour levels are used in the three plots. (a) Standard HYSCORE, pulse sequence $16-\tau-16-t_1-16-t_2-16-\tau-$echo, τ = 144 ns. (b) Proton-matched HYSCORE, pulse sequence $16-\tau-72(HTA)-t_1-16-t_2-72(HTA)-\tau-$echo, $\omega_{1S}/2\pi$ = 14.7 MHz, τ = 144 ns. (c) Nitrogen-matched HYSCORE, pulse sequence $16-\tau-72(HTA)-t_1-16-t_2-72(HTA)-\tau-$echo, $\omega_{1S}/2\pi$ = 30 MHz, τ = 136 ns.

levels are chosen with an exponentially increasing spacing (2^n law) from a lowest level just above the noise. The most prominent peaks are labeled by numbers (only half of the transitions; the other half is symmetric to the diagonal): basic frequency peaks: {1}: ($\omega_{\alpha1}$, $\omega_{\beta1}$), strong matrix line of a large number of weakly coupled protons; {2}: ($\omega_{\alpha2}$, $\omega_{\beta2}$), proton peak with $A_2/2\pi$ = 3 MHz; {3}: ($\omega_{\alpha3}$, $\omega_{\beta3}$), very strong proton peak with $A_3/2\pi$ = 4.5 MHz; {4}: ($\omega_{\alpha4}$, $\omega_{\beta4}$), proton peak with $A_4/2\pi$ = 6.8 MHz; combination frequency peaks: {5}: ($2\omega_{\alpha1}$, $2\omega_{\beta1}$); {6}: ($\omega_{\beta3}$, $2\omega_{\alpha3}$); {7}: ($\omega_{\alpha3}$, $2\omega_{\beta3}$); {8}: ($2\omega_{\alpha3}$, $2\omega_{\beta3}$), peaks 6–8 indicate that two equivalent protons exist; {9}: ($\omega_{\beta1}$, $\omega_{\alpha3}$ + $\omega_{\alpha1}$); {10}: ($\omega_{\alpha1}$, $\omega_{\beta1}$ + $\omega_{\beta3}$); {11}: ($\omega_{\alpha1}$ + $\omega_{\alpha3}$, $\omega_{\beta1}$ + $\omega_{\beta3}$); {12}: ($2\omega_{\alpha1}$, $2\omega_{\beta3}$); cross peak within the same m_S manifold: {13}: ($\omega_{\beta3}$, $2\omega_{\beta3}$), tentative assignment, this type of cross peak can be generated by a π pulse that is not sufficiently nonselective; {14}–{19}: peaks of a weakly coupled nitrogen of $Ni(sal)_2$ and combination of it with protons (tentative assignment); {20}: ^{13}C diagonal peak (natural abundance). The peaks along the diagonal are caused by a π pulse that is not sufficiently nonselective. Note that for sensitivity reasons, only combination peaks with proton {3} are observed. Figure 10 shows the surface plots of the antidiagonal at 24.8 MHz of the standard and the proton-matched HYSCORE spectrum ({5}, {8}, and {11} in Fig. 9). Note the shoulders of the matrix sum combination peak {5} that is resolved in the combination frequency region but not in the basic frequency region of the spectrum. In the standard HYSCORE experiment, these lines, except peak {8}, are below the noise level.

In Fig. 11 the nitrogen region obtained with standard HYSCORE is compared with nitrogen-matched HYSCORE. For these two magnetically equivalent nitrogens, the peak amplitudes are *more than one order of magnitude* larger in the matched experiment (Fig. 11b, contour levels 8–80) than in the standard experiment (Fig. 11a, contour levels 1–6). The first-order transition frequencies for one nitrogen are given by $\omega_{\alpha1} = A_N/2 + \omega_{IN} + \frac{3}{2}Q_N$ ($m_S = \frac{1}{2}$, m_I: $1 \leftrightarrow 0$), $\omega_{\alpha2} = A_N/2 + \omega_{IN} - \frac{3}{2}Q_N$ ($\frac{1}{2}$, $0 \leftrightarrow -1$), and $\omega_{\beta1} = A_N/2 - \omega_{IN} - \frac{3}{2}Q_N$ ($-\frac{1}{2}$, $0 \leftrightarrow 1$), $\omega_{\beta2} = A_N/2 - \omega_{IN} + \frac{3}{2}Q_N$ ($-\frac{1}{2}$, $-1 \leftrightarrow 0$). Here A_N and Q_N denote the hyperfine and quadrupole coupling for this particular crystal orientation, respectively. The prominent cross peaks along the antidiagonal are {1}, ($\omega_{\alpha1}$, $\omega_{\beta1}$); and {2}, ($\omega_{\alpha2}$, $\omega_{\beta2}$), ($\omega_{\beta1}$, $\omega_{\alpha1}$), and ($\omega_{\beta2}$, $\omega_{\alpha2}$). The weaker cross peaks are assigned to {3}, ($\omega_{\alpha2}$, $\omega_{\beta1}$); and {4}, ($\omega_{\alpha1}$, $\omega_{\beta2}$), ($\omega_{\beta1}$, $\omega_{\alpha2}$), and ($\omega_{\beta2}$, $\omega_{\alpha1}$) (observed with lower contour levels). Since the peaks {1}–{4} are arranged in a square, peaks {1} and {2} belong to the same m_S manifold. Second-order splittings that can sometimes be observed in ENDOR experiments in systems with magnetically equivalent nitrogen nuclei (*30, 32*) are not resolved. With $\omega_{IN}/2\pi = -0.89$ MHz we then find for this particular crystal orientation for the coupling parameters of the nitrogen $A_N/2\pi$ = 44.6 MHz and $|Q_N|/2\pi$ = 0.44 MHz.

CONCLUSION

We introduced pulse matching as a tool for sensitivity enhancement in three-pulse ESEEM and HYSCORE experiments. All the paramagnetic species that have been subjected to a matched-pulse experiment showed a signal-to-noise improvement of at least a factor of 2, and in many cases an increase in signal intensity by more than one order of magnitude was obtained. In matched three-pulse ESEEM, the effect was found to be less pronounced than in HYSCORE. In matched HYSCORE, the sensitivity improvement is often overwhelming, for both strongly coupled nuclei with a pre-

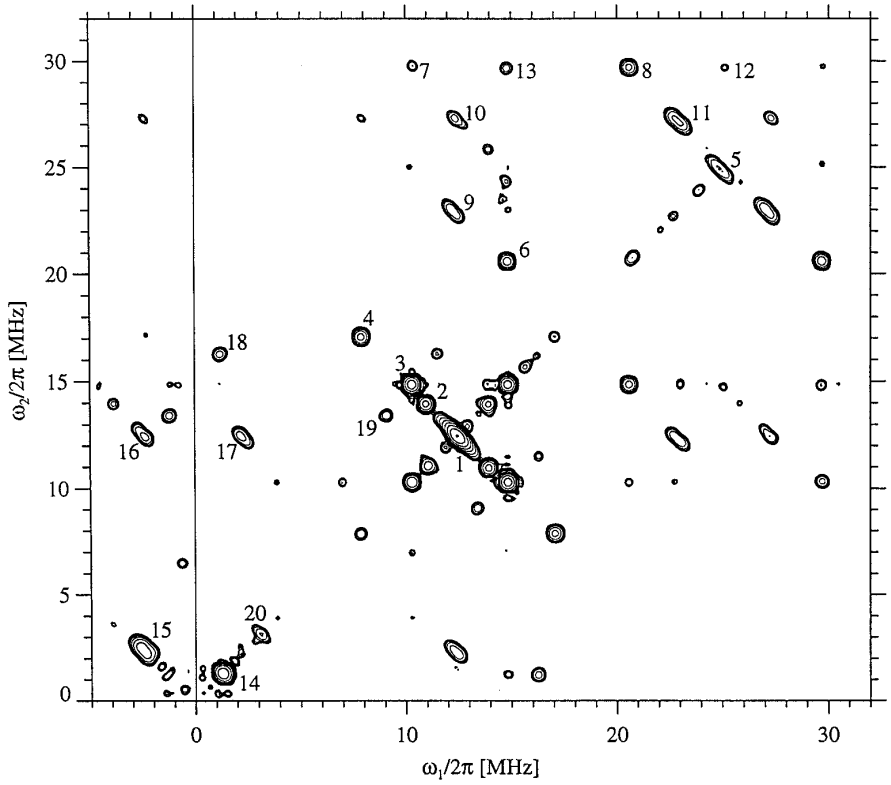

FIG. 9. Contour plot of the proton-matched HYSCORE spectrum of $Cu(sal)_2$, logarithmic contour levels. First quadrant and part of the second quadrant. For assignment of the numbered cross peaks, see text.

dominantly isotropic hyperfine interaction and weakly coupled nuclei with a small depth parameter k. This is particularly true for combination frequencies where n-quantum coherences are involved with nuclear modulation amplitudes proportional to k^n. It has been demonstrated that in favorable cases the combination frequency peaks allow a ''counting'' of the number of nuclei surrounding the unpaired electron.

The implementation of matched-pulse EPR experiments is very simple and straightforward. To perform a matched-pulse experiment, one has only to match some of the pulses roughly to the nuclear Zeeman frequency in the weak coupling case, or to apply the maximum available mw field strength in the strong coupling case, and to use proper pulse lengths.

Matched pulses can be used in 1D and 2D pulse EPR experiments where nuclear coherence is created and is trans-

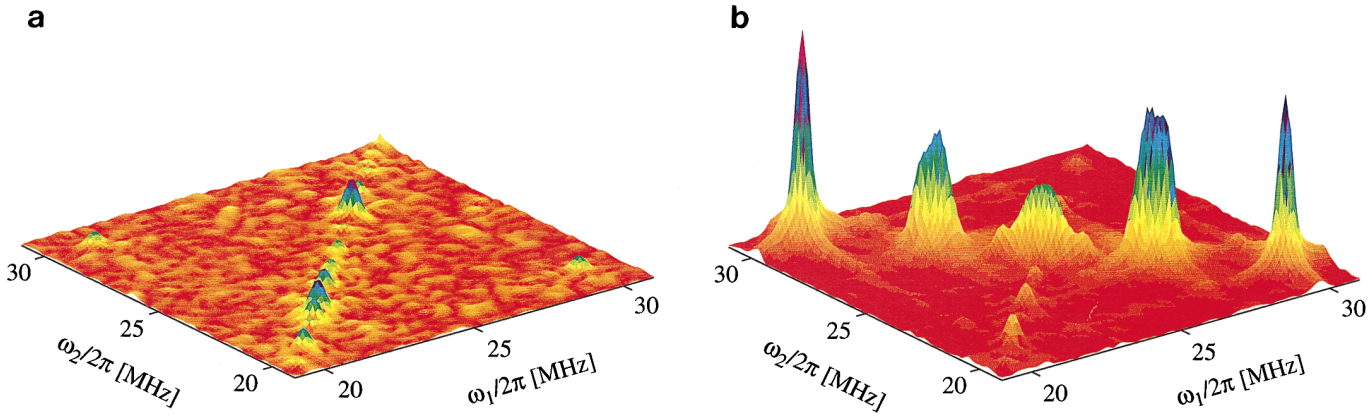

FIG. 10. Surface plots of the proton double-quantum region. (a) Standard HYSCORE. (b) Proton-matched HYSCORE.

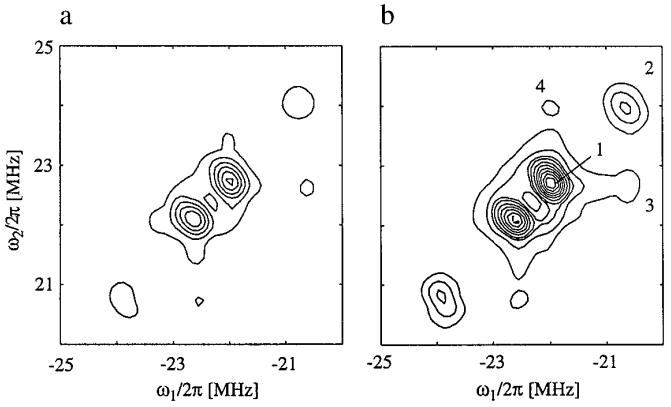

FIG. 11. Nitrogen region of the HYSCORE spectrum of $Cu(sal)_2$. (a) Standard HYSCORE. (b) Nitrogen-matched HYSCORE. The lowest contour level and the steps between the contours are eight times larger than those in (a). For assignment of the numbered cross peaks, see text.

ferred to electron coherence for indirect detection. In particular in DONUT-HYSCORE (*do*uble *nu*clear coherence *t*ransfer HYSCORE) (*33*), a new 2D ESEEM experiment for correlating nuclear frequencies within the *same* m_S manifold, the concept of matched pulses increases the intensity of cross peaks of transitions with small depth parameters drastically (*34*).

ACKNOWLEDGMENTS

This research has been supported by the Swiss National Science Foundation. The preparation of some of the 2D plots by Jaap Shane is gratefully acknowledged. We thank Professor E. S. Nefed'ev from Kazan State Technological University, Kazan, Russia, for the expoxy adhesive.

REFERENCES

1. W. B. Mims, *Phys. Rev. B* **5,** 2409 (1972).
2. S. A. Dikanov and Yu. D. Tsvetkov, ''Electron Spin Echo Envelope Modulation Spectroscopy,'' CRC Press, Boca Raton, FL (1992).
3. A. Schweiger, *in* ''Modern Pulsed and Continuous-Wave Electron Spin Resonance'' (L. Kevan and M. Bowman, Eds.), p. 43, Wiley, New York (1990).
4. P. Höfer, A. Grupp, H. Nebenführ, and M. Mehring, *Chem. Phys. Lett.* **132,** 279 (1986).
5. J. J. Shane, P. Höfer, E. J. Reijerse, and E. de Boer, *J. Magn. Reson.* **99,** 596 (1992).
6. P. Höfer, *J. Magn. Reson. A* **111,** 77 (1995).
7. C. Gemperle, G. Aebli, A. Schweiger, and R. R. Ernst, *J. Magn. Reson.* **88,** 241 (1990).
8. A. Ponti and A. Schweiger, *J. Chem. Phys.* **102,** 5207 (1995).
9. M. Hubrich, G. Jeschke, and A. Schweiger, *J. Chem. Phys.* **104,** 2172 (1996).
10. A. Pöppl, R. Böttcher, and G. Völkel, *J. Magn. Reson. A* **120,** 214 (1996).
11. C. Gemperle, A. Schweiger, and R. R. Ernst, *Chem. Phys. Lett.* **178,** 565 (1991).
12. Th. Wacker and A. Schweiger, *Chem. Phys. Lett.* **186,** 27 (1991).
13. E. J. Hustedt, A. Schweiger, and R. R. Ernst, *J. Chem. Phys.* **96,** 4954 (1992).
14. R. Song, Y. C. Zhong, C. J. Noble, J. R. Pilbrow, and D. R. Hutton, *Chem. Phys. Lett.* **237,** 86 (1995).
15. G. Jeschke and A. Schweiger, *Mol. Phys.* **88,** 355 (1996).
16. S. R. Hartmann and E. L. Hahn, *Phys. Rev.* **128,** 2042 (1962).
17. L. Müller and R. R. Ernst, *Mol. Phys.* **38,** 963 (1979).
18. H. Brunner, R. H. Fritsch, and K. H. Hausser, *Z. Naturforsch. A* **42,** 1456 (1987).
19. A. Henstra, P. Dirksen, J. Schmidt, and W. Th. Wenckebach, *J. Magn. Reson.* **77,** 389 (1988).
20. G. Jeschke and A. Schweiger, *J. Chem. Phys.* **105,** 2199 (1996).
21. G. Jeschke and A. Schweiger, *J. Chem. Phys.* **106,** 9979 (1997).
22. S. A. Smith, T. O. Levante, B. H. Meier, and R. R. Ernst, *J. Magn. Reson. A* **106,** 75 (1994).
23. L. Kevan, M. K. Bowman, P. A. Marayama, R. K. Boukman, V. F. Yudanov, and Yu. D. Tsvetkov, *J. Chem. Phys.* **63,** 409 (1975).
24. Ichikawa, L. Kevan, M. K. Bowman, S. A. Dikanov, and Yu. D. Tsvetkov, *J. Chem. Phys.* **71,** 1167 (1979).
25. L. Kevan, *in* ''Time Domain Electron Spin Resonance'' (L. Kevan and R. N. Schwartz, Eds.), p. 279, Wiley–Interscience, New York (1979).
26. K. P. Dinse, R. Biehl, and K. Möbius, *J. Chem. Phys.* **61,** 4335 (1974).
27. M. Mehring, P. Höfer, and A. Grupp, *Ber. Bunsen-Ges. Phys. Chem.* **91,** 1132 (1987).
28. A. Schweiger, *Angew. Chem. Int. Ed. Engl.* **30,** 265 (1991).
29. E. S. Nefed'ev, M. K. Kadirov, N. V. Chuikova, S. B. Orlinskii, and R. M. Rakhmatullin, *in* ''Electron Spin Resonance in Electron Transfer and Organic Solids,'' Abstracts, p. P24, Dresden (1995).
30. A. Schweiger and Hs. H. Günthard, *Chem. Phys.* **32,** 35 (1978).
31. R. R. Ernst, G. Bodenhausen, and A. Wokaun, ''Principles of Nuclear Magnetic Resonance in One and Two Dimensions,'' Clarendon Press, Oxford (1987).
32. A. Schweiger, F. Graf, G. Rist, and Hs. H. Günthard, *Chem. Phys.* **17,** 155 (1976).
33. R. Rakhmatullin, D. Goldfarb, and A. Schweiger, to be published.
34. L. Liesum, R. Rakhmatullin, and A. Schweiger, to be published.